



Photocatalytic indoor/outdoor air treatment and bacterial inactivation on $\text{Cu}_x\text{O}/\text{TiO}_2$ prepared by HiPIMS on polyester cloth under low intensity visible light



M. Abidi^{a,b}, A.A. Assadi^{a,*}, A. Bouzaza^a, A. Hajjaji^b, B. Bessais^b, S. Rtimi^{c,*}

^a Univ Rennes, Ecole Nationale Supérieure de Chimie de Rennes, CNRS, ISCR (Institut des Sciences Chimiques de Rennes), UMR 6226, F-35000 Rennes, France

^b Laboratoire de Photovoltaïque, Centre de Recherches et des Technologies de l'Energie, Technopole de Borj-Cédria, BP 95, 2050 Hammam-Lif, Tunisia

^c Ecole Polytechnique Fédérale de Lausanne, 1015 Lausanne, Switzerland

ARTICLE INFO

Keywords:
 Photocatalysis
 HiPIMS coating
 VOC elimination
 Bacterial inactivation
 Redox catalysis

ABSTRACT

In this study, photoactive $\text{Cu}_x\text{O}/\text{TiO}_2$ coatings were prepared using magnetron sputtering operated at different powers and modes (Direct-current magnetron sputtering and High Power Impulse magnetron sputtering). Indoor/outdoor air pollutions (Volatile Organic Compounds, VOCs) degradation have been dramatically reduced on sputtered $\text{Cu}_x\text{O}/\text{TiO}_2$ on polyester (PES) cloth under low intensity visible light. The Low intensity visible light was used to irradiate the sputtered photocatalysts, which degraded various VOC molecules concomitant with a bacterial inactivation ability. The VOC removal kinetics were studied in the dark and under visible light as a function of the deposition time and applied peak currents during the coating by HiPIMS. High concentrations of chloroform and butyraldehyde were shown to be degraded (90% and 85%, respectively) on $\text{Cu}_x\text{O}/\text{TiO}_2$ -PES fabrics under daylight irradiation. The repetitive reuse of the sputtered coatings was also investigated showing the long operational lifetime of the prepared fabrics. The deposition rates of Ti and Cu atoms and their atomic distribution along the sputtered film have been investigated by Transmission Electronic Microscopy (TEM). Redox catalysis was shown to happen within the VOC degradation time as detected by X-ray Photoelectron Spectroscopy (XPS). Deconvolution of the $\text{Cu}2\text{p}3/2$ peak in the $\text{Cu}_x\text{O}/\text{TiO}_2$ on PES samples showed changes in the Cu_2O and CuO within the VOCs degradation and the bacterial inactivation. The interfacial charge transfer (IFCT) between Cu_xO induced under light leading to VOCs oxidation path seemed to require a low photons energy and were able to oxidize the pollutants even at high concentrations. The mechanisms involving the VOCs degradation on $\text{Cu}_x\text{O}/\text{TiO}_2$ catalysts are suggested in which the holes generated by Cu_2O transfer to TiO_2 in the $\text{TiO}_2(\text{n})/\text{Cu}_x\text{O}(\text{p})$ in the hetero-junction. This transfer is favored by the electrostatic interaction between both semiconductors. The photo-generated ROS, mainly $\cdot\text{OH}$ -radicals were determined by fluorescence method. The possible contribution of the $\cdot\text{OH}$ -radicals in the bacterial inactivation on the sputtered $\text{Cu}_x\text{O}/\text{TiO}_2$ catalysts was discussed. DRS, TEM, contact angle (CA) and XPS were used to characterize the catalyst optical and structural properties.

1. Introduction

Volatile Organic Compounds (VOCs) became of a huge concern to the social, economic and scientific community as it presents a huge issue that threatens the sustainability of ecosystems and the well-being of both fauna and flora [1,2]. European Environmental Agency estimated that Europeans spend 90% of their time indoor [3]. Americans and Canadians spend 87% of time indoor and an additional 6% in a vehicle [4]. In fact, many reports have emphasized on the hazardous aspect of these compounds, since their presence in the atmosphere could lead to

serious respiratory problems for humans and animals [2,5,6], significantly decreases crops production yield and causes an unpleasant mist especially in mega-cities and industrial areas [3–7].

In this context, an important attention has been paid for the treatment of industrial emitted gases in order to carry on with the important growth that this sector has witnessed during the last decades in terms of goods production and resources consumption [7]. A variety of techniques was highlighted in order to reduce the amount of organic pollution in the air, namely adsorption [8], condensation [9], plasma combined with catalysis [10–12], incineration and thermic combustion [9] and

* Corresponding authors.

E-mail addresses: aymen.assadi@ensc-rennes.fr (A.A. Assadi), sami.rtimi@epfl.ch (S. Rtimi).

biological degradation [13]. Despite their considerable efficiency in the elimination of VOCs, these techniques were shown to generate high amounts of hazardous by-products and sludge and in some cases only presents a temporary pollution transfer from gaseous to solid phase [14] or from one place to another.

Among these techniques, heterogeneous photocatalysis was considered as a clean technology for air depollution due to its capacity to eliminate VOCs with high efficiency [15,16], leading to their complete mineralization without a significant production of possibly harmful oxidation by-products [11,17]. However, the majority of the elaborated studies reported the exorbitant amount of energy that has been consumed during the run of the photocatalytic processes [18–22] as well as the unsuitability of these techniques for a certain industrial requirement [21]. Furthermore, the classically used catalyst, TiO_2 on glass fiber tissue [23,24], TiO_2 on cellulosic paper [19], TiO_2 on polymer support [23] and TiO_2 on PES fabrics [27,24,25] did not offer a pertinent purification capacity of the effluent under visible light and needed to be further improved in order to reach higher mineralization levels [19,23,26]. Hence, the shifting of photocatalytic processes to the use of visible light on metal-doped semiconductors was highlighted by recent studies reporting encouraging results in the treatment of gas emissions and dye-loaded industrial wastewater effluents [22–27]. Indeed, the use of visible light in presence of metal-doped semiconductors can lead to improve the efficiency of VOCs degradation and microorganisms [29–32].

During the last few years, many research groups focused on the preparation of innovative catalysts for bacterial inactivation [33]. Wang et al., reported on the antibacterial behavior of CuI - BiOI / Cu films prepared by water bath method and their enhanced photo-induced charge separation under visible-light [34]. The same research group reported on the role of the photogenerated h^+ , e^- and O_2^- playing synergistic effect for the photocatalytic disinfection over Ag @ AgI / Bi - BiOI three-dimensional nano-architectures [35]. Many efforts are running today for the design of Lotus effect self-cleaning/self-sterilizing coatings for hospital textile [28–30].

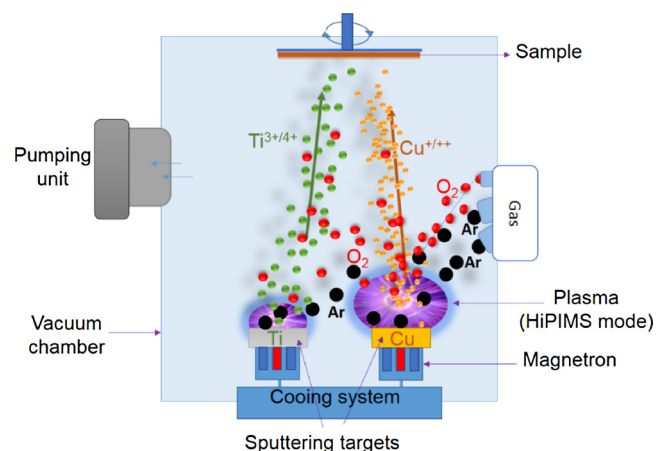
The aim of the present work is to explore the removal efficiency of indoor air pollutants such butyraldehyde (from now as BUTY) and chloroform in batch reactor on $\text{Cu}_x\text{O}/\text{TiO}_2$ sputtered on PES. The influence of inlet concentration and catalyst on the pollutant removal are investigated in details. In addition to the indoor air pollutants, the sputtered fabrics were tested for the chloroform removal. Moreover, an interesting challenge of this work is to study also the effect of the preparation conditions on the photocatalytic inactivation of *E. coli*. The photocatalyst were characterized by up-to-date surface science techniques.

2. Material and methods

2.1. $\text{Cu}_x\text{O}/\text{TiO}_2$ sputtered PES

The $\text{Cu}_x\text{O}/\text{TiO}_2$ coatings were sputtered using combined reactive DCMS/HiPIMS process. Ti target was operated under DCMS mode and Cu target (99.99% pure) was operated using reactive HiPIMS mode. The sputtering chamber was operated at a high vacuum with a residual pressure $< 4 \times 10^{-5}$ Pa equipped with two confocal targets 5 cm in diameter (Lesker. Hastings, East Sussex pure). A HiP3 5kW Solvix generator was used for the HiPIMS deposition and was operated at an average power of 100 W (5 W cm^{-2}) with a pulse-width of 50 μs and a frequency of 1 KHz. The gas phase inside the sputtering chamber was 95% Ar : 5% O_2 . The DC power in the second target was performed at 90 W for the first 30 s then at 50 W to adjust the relative content of Ti in the film as it will be shown later by high-resolution transmission electron microscopy. A TiO_2 under layer was puttered before the Cu_xO deposition. The target-to-substrate distance was fixed at 10 cm as shown in **Scheme 1** below.

The low surface energy of PES cloth can lead to poor sputtered



Scheme 1. Illustration of the sputtering unit used to prepare the photocatalyst used in the present study.

nanoparticles' adhesion. In order to increase the uniform distribution of Cu on PES, an under layer of TiO_2 was sputtered for 20 s followed by the Cu deposition (from a separate target). The latter plays the role of stabilizer to Cu species as previously reported [37,38]. In addition, the presence of TiO_2 reduces the aggregation of Cu on the substrate surface [39]. Furthermore, the PES fabrics were pretreated by UVC-light (15 min) to induce a higher density of functional polar groups able to bind the sputtered Ti-species [28,29,36,37]. UVC irradiation was carried out using a 185/254 nm low-pressure mercury lamp (Ebara Corp., Tokyo, Japan). The UVC lamp (25 W) presented emission lines at 185 nm and 254 nm in a ratio 1:4.

2.2. Materials and chemicals

Photocatalytic experiments were performed using a cylindrical batch reactor, 10 mm as upper diameter and 50 mm of working height, thus accepting up to 50 mL of the studied pollutant. A fluorescent visible lamp could be inserted inside the reactor from above. The reactor contains two septum; one of them is used for samples extractions (Fig. 1). The photon excitation was provided by a Sylvania CF-L 24 W/ 840 source with a spectral emission in visible range (400–720 nm). This light source is similar to light used for hospital facilities, schools and houses. This is the reason why we are calling it as "indoor light". The spectral emission of the lamp is illustrated in Fig. 1. The whole micro-reactor was covered with an aluminum thin layer to prevent visible emission. A magnetic stirrer and barrel allows the gas phase to be homogenized.

The $\text{Cu}_x\text{O}/\text{TiO}_2$ -PES samples were placed in the inner space of the tube to be in direct contact with the studied gas and the light radiation. The surface of the catalyst was constant of about 20 cm^2 for all the carried experiments.

2.3. Photocatalytic tests and analytical tools

In order to test the photocatalytic performance, a common volatile organic compound was used, chloroform. Analysis of Chloroform/BUTY was performed using a gas chromatography gas phase (Fisons GC9000) equipped with a flame ionization detector (FID). Nitrogen is the carrier gas and constitutes the mobile phase. All injections were performed manually with a syringe of 500 μL and repeated at least three times.

The pollutants analysis can only start once the airflow in the reactor reaches equilibrium. A certain time is required after the pollutant is injected in the reactor, so that its concentration stabilizes. Once the outlet concentration is stabilized and the catalyst is loaded, light is on and the photocatalytic oxidation starts.

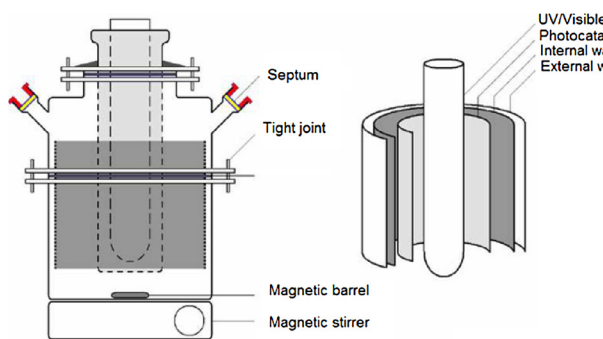


Fig. 1. Schematic of the batch photo-reactor with the central co-axial Sylvania CF-L 24 W/840 light source (400–720 nm).

2.4. Bacterial inactivation tests and ·OH-radical identification

The evaluation of the bacterial inactivation was carried out by plate counting agar method. The *Escherichia coli* (*E. coli* K12) was obtained from the Deutsche Sammlung von Mikro-organismen und Zellkulturen GmbH (DSMZ), Braunschweig, Germany to test the sputtered samples bacterial inactivation. The sputtered PES fabrics were sterilized keeping them at 70 °C overnight. Aliquots of 50 µL bacterial culture suspended in NaCl/KCl (8 g/l NaCl and 0.8 g/l KCl) solution with a concentration of 8×10^5 colony forming unit per milliliter (CFU. mL⁻¹) were placed on sputtered and unspotted (control) PES samples. The samples were placed in Petri dishes provided with a lid to prevent evaporation. At preselected times, the samples were transferred into a sterile 2 mL Eppendorf tube containing autoclaved NaCl/KCl saline solution. These solutions were subsequently mixed thoroughly using a Vortex. Serial dilutions were made in NaCl/KCl solution taking 100 µL aliquots. Then 100 µL aliquots were pipetted onto a nutrient agar plate, for the bacterial counting by the standard plate method. These agar plates were incubated, lid down, at 37 °C for 24 h before colonies counting. The bacterial tests reported in this study were carried out in triplicates. To verify that no re-growth of *E. coli* occurs after the first bacterial inactivation cycle, the sputtered films were incubated on an agar Petri dish at 37 °C for 24 h. Statistical analysis are presented by mean of standard deviation (n = 5%).

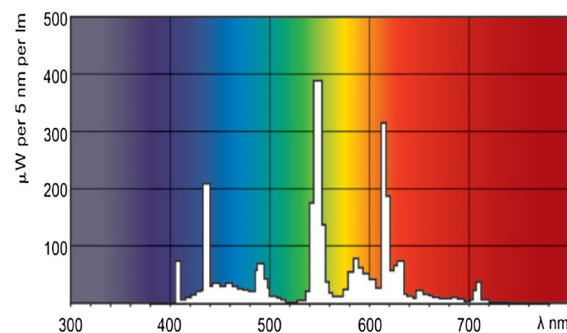
For the quantification of the ·OH-radical, samples of 9 cm² were immersed in a solution of terephthalic acid (0.4 mmol L⁻¹) dissolved in NaOH (4 mmol L⁻¹). After preselected irradiation times, the solution was transferred in a quartz cell. The fluorescence of the photo-generated 2-hydroxyterephthalic-acid was quantitatively monitored on a Perkin Elmer spectrometer. The spectra were recorded at a scan rate of 100 nm/min after excitation at 315 nm.

2.5. Cu_xO/TiO₂ Characterization: Thickness, TEM, CA, spectral absorption and XPS

Thicknesses of the TiO₂, Cu_xO and Cu_xO/TiO₂ thin films were measured by profilometry (Alphastep-500, Tencor, USA) after deposition on Si-wafers. To be able to perform the transmission electron microscopy (TEM), the PES fabrics were embedded in epoxy resin (Embed 812) and cross-sectioned with an ultra-microtome (Ultracut E) up to thin layers of 80–100 nm thick. These thin layers were then placed on TEM holey carbon grid in order to image the samples. The spot size was set to 5 µm, dwell time 50 µs and the real time of 600 s. The contact angles (CA) of TiO₂, Cu_xO/TiO₂ were determined by the sessile drop method on a Data Physics OCA 35 unit.

Diffuse reflectance spectroscopy (DRS) of TiO₂, Cu_xO and Cu_xO/TiO₂ was carried out a Perkin Elmer Lambda 900 UV-VIS-NIR spectrometer within the wavelength range of 250–750 nm. The background was subtracted using an unspotted PES fabric. Optical spectra were analyzed by the Tauc's method.

An AXIS NOVA photoelectron spectrometer (Kratos Analytical,



Manchester, UK) provided for with monochromatic AlKa ($\hbar\nu = 1486.6$ eV) anode. Binding energies (BE) were calibrated against the standard C1s binding energy at 284.6 eV [27,28]. A Multipak (version 9 software) using 70:30 Gaussian: Lorentzian peak shape and a Shirley background function were used for Spectra deconvolution as previously reported [28,29,36,37].

3. Results and discussion

3.1. Thickness calibration and TEM of sputtered Cu_xO/TiO₂-PES

The thickness calibration of the Cu_xO deposited by HiPIMS at 20, 40 and 80 A on Si-wafer was investigated. Sputtering Cu_xO for 100 s at 100 A led to a layer of ~70 nm thick. This is equivalent to 350 atomic layers, each containing 10^{15} Cu-atoms/cm² being deposited at a rate of $\sim 5 \times 10^{15}$ atom/cm²s [38].

The PES fabrics were initially pretreated with UVC for 15 min as previously described. UVC pretreatment enhances the polarity, roughness and hydrophilicity of polyester improving the interfacial adhesion of TiO₂ as previously reported by Kiwi et al. [39] and R.A. Jelil [41]. The UVC pre-treatment induced negatively charged functional groups, e.g., carboxylic, percarboxylic, epoxide and peroxide groups due to the atomic and excited O [26]. The PES negative sites bind the positive ions generated in the plasma phase Ti⁴⁺/Ti³⁺/Cu⁺/Cu²⁺. This involves electrostatic attractions including chelation/complexation [36]. The TiO₂ was deposited immediately after the UVC pretreatment due to the short lifetimes of the polar radical species.

Transmission electron microscopy (TEM) images of the sputtered Cu_xO/TiO₂ on PES shows a continuous coating of TiO₂ under layer on PES fabrics. TiO₂ thickness of 10–15 nm is equivalent to 50 atomic layers [26], taking an atomic layer thickness of 0.2 nm [39]. During the deposition of the TiO₂ under layer and the Cu_xO, the Ar/O₂ ratio was fixed at 19. The oxygen atoms distribution shows the oxide nature of the Ti and the Cu upper layer. Uniform distribution of Cu-species on the TiO₂ under layer with a high oxygen content. This reveals the oxidation of both under and upper layers during the deposition. Table 1 shows the Ti, O and Cu weight and atomic percentages in the sputtered films as determined by EDX.

The Cu_xO layer uniformity and particulates shape/size are dependent on the number of deposited atomic layers. This controls the structure-reactivity relation of the Cu-catalyst clusters sputtered on the

Table 1
EDX area and elemental mapping analysis of Cu_xO-TiO₂-PES both sputtered for 100 s at 80 A.

Element	Weight %	Atomic %
O K	16.53	68.73
Ti K	3.66	4.41
Cu K	54.3	17.47

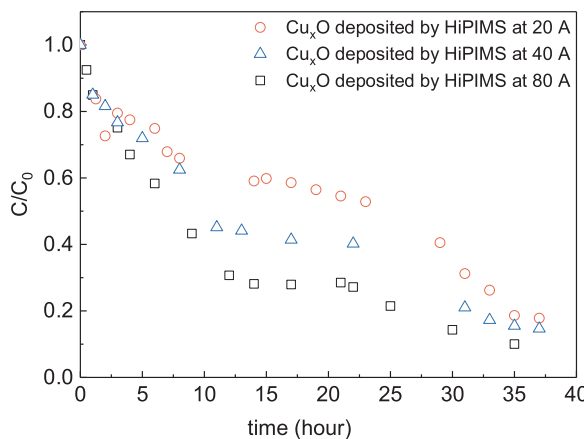


Fig. 2. Removal of chloroform with catalyst $\text{Cu}_x\text{O}/\text{TiO}_2\text{-PES}$ at different HiPIMS sputtering currents deposited for 100 s.

PES-substrate [42,43]. Both layers were deposited in reactive mode in the presence of oxygen. In addition, the exposition of the sample to ambient environment after preparation can lead to further oxidation of the top-most layers as reported previously [28–30,37].

3.2. Photocatalytic experiments

3.2.1. Effect of the deposition Current of Cu_xO on $\text{TiO}_2\text{-PES}$ on the photocatalytic activity under low intensity light: Chloroform removal

Fig. 2 shows the chloroform removal on $\text{Cu}_x\text{O}/\text{TiO}_2\text{-PES}$ sputtered for 20, 80 and 100 A. It is readily seen from Fig. 2 that $\text{Cu}_x\text{O}/\text{TiO}_2\text{-PES}$ photocatalyst sputtered at 80 A led to the fastest chloroform removal compared to samples sputtered at 20 and 100 A. An increase in sputtering current from 20 to 80 A led to two times increase in the chloroform removal (from 40 to 72% of the initial 6 mg/m^3 of chloroform). This is due to the availability of the photocatalytic sites generated at the interface of the sample deposited at (80A). At low current values, the degradation will tend to a limit. It was recently reported that the deposition current in HiPIMS generates different ions/charged species [44]. This leads to differentiate charges at the thin films interface.

3.2.2. Effect of the deposition time of Cu_xO on $\text{TiO}_2\text{-PES}$ on their photocatalytic activities

The photocatalytic activities of Cu_xO deposited for different time (5, 20 and 100 s) on TiO_2 under layer were investigated in details. For the copper-based photocatalyst (Fig. 3) and when comparing different

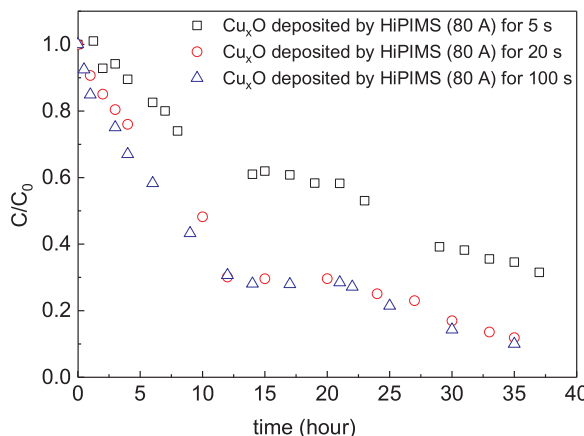


Fig. 3. Removal of chloroform on HiPIMS-sputtered $\text{Cu}_x\text{O}/\text{TiO}_2\text{-PES}$ (at 80 A) deposited at different times.

times of deposition under low intensity light, it is readily seen that the degradation of chloroform was significantly affected by the deposition time of Cu_xO and thus its amount on the surface. Indeed, the normalized concentrations of chloroform shown in Fig. 3 decreased up to 71% within 15 h irradiation. This result is in agreement with other results reported for some other VOCs [38,26].

It has been recently reported that the thickness/amount and microstructure of Cu are a function of the applied sputtering current and lead to the significant difference in the total-ions count [42]. Recent reports investigated the ions distribution from the plasma phase (inside the magnetron sputtering chamber) until the resulting Cu_xO thin film (before and after exposition to light) [44]. S. Konstantinidis et al., reported on the diagnostics and understanding of the plasma–surface interaction in HiPIMS discharges [45–47]. The same authors followed the deposition rate of TiO_2 films as a function of the applied current and showed that the deposition rate increases until a certain current intensity then it decreases [46]. This can explain the lower photocatalytic activity observed for the sample sputtered at 100 A. Similar trends was observed by Kiwi et al., and was attributed to the inward charge diffusion in thick catalytic films [48–51].

The chloroform removal on $\text{Cu}_x\text{O}/\text{TiO}_2\text{-PES}$ with 100 s of sputtering time was about twice time faster compared to the same catalyst with 5 s of sputtering time; it reaches 80% removal in 12 h with 20 s of sputtering as seen in Fig. 3. On $\text{Cu}_x\text{O}/\text{TiO}_2\text{-PES}$, only 40% of 6 mg/m^3 of chloroform were removed within same period. This observation can be explained by the fact that 5 s is very low to form a layer of catalyst leading to chloroform degradation.

On other way, we see that increasing the time sputtering from 20 to 100 s has no effect of VOC removal. In fact, we note the same removal of chloroform. This observation is due to the fact that chloroform molecules adsorption is mainly a monolayer process and the increase in deposit time is considered could be associated to a multilayer coating thickness of the catalyst [28]. Similar results were recently reported [40] when investigating bacteria degradation using TiO_2 in water. Analysis results were discussed according to the variation of deposition time and used galvanostatic current intensity during pulverization process.

3.2.3. Effects of indoor/outdoor pollutants on $\text{Cu}_x\text{O}/\text{TiO}_2\text{-PES}$ performance

Fig. 4 shows that under 80 A and with visible light, the degradation of two kinds of pollutants, with equimolar inlet concentration, is quiet similar. However, when we decrease the intensity of light (data not shown), we observed that the degradation of chloroform is becoming slower than that of butyraldehyde. Therefore, we can conclude that the copper-based catalyst is more efficient for the degradation of

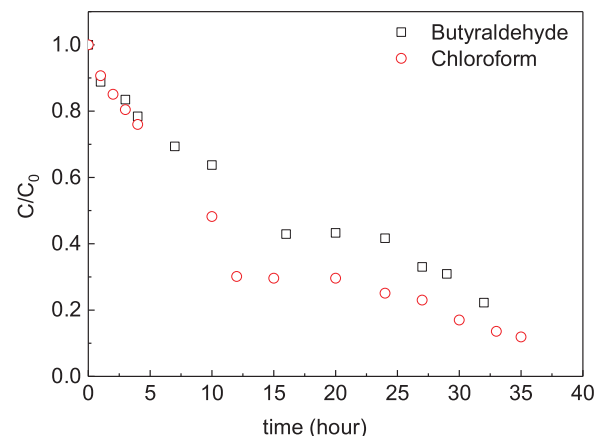


Fig. 4. Indoor/outdoor pollutants removal on $\text{Cu}_x\text{O}/\text{TiO}_2\text{-PES}$ HiPIMS-sputtered 80 A for 20 s under a visible lamp irradiation.

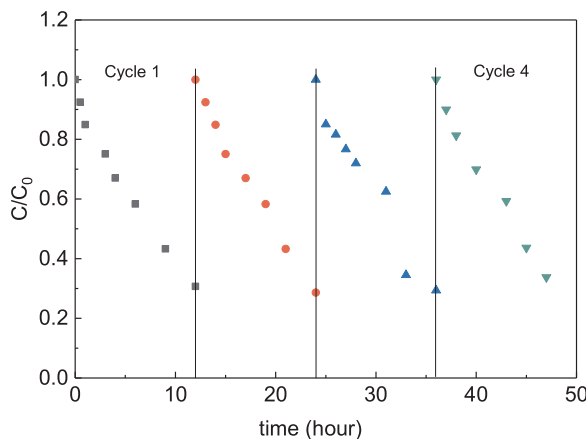


Fig. 5. Degradation profile of chloroform with photocatalysis on a $\text{Cu}_x\text{O}/\text{TiO}_2$ -PES sample under visible light. Further experimental conditions: $I = 30\text{W/m}^2$, Chloroform concentration = 6 g/m^3 .

butyraldehyde.

After 10 h visible light illumination, the photocatalytic removal kinetics of chloroform was faster than butyraldehyde. This can be due to the chemical properties of pollutants, their affinities towards the catalyst and the accumulation of their intermediate by-products on the surface of catalyst leading to competition effect of VOC towards the catalytic active sites.

3.3. $\text{Cu}_x\text{O}/\text{TiO}_2$ -PES catalyst recyclability

The reusability of the tested samples is an important factor to investigate since it is a measure for its practical application potential degrading pollutants in the gas phase [39,40]. To investigate the applicability of the developed copper sample to operate in four successive cycles, several visible photocatalytic oxidations were done. The copper catalyst was thoroughly washed after each photodegradation cycle and reused. The results of repetitive use of the $\text{Cu}_x\text{O}/\text{TiO}_2$ -PES photocatalyst up to the 4th cycle is shown below in Fig. 5. We note no loss of sample photo-activity. The results reported in Fig. 5 show the overall potential of the $\text{Cu}_x\text{O}/\text{TiO}_2$ -PES samples for application in air treatment. We note the same slope of the removal rate during each cycle. Thus, this behavior can confirm the no deactivation of surface sites and an excellent catalytic stability of $\text{Cu}_x\text{O}/\text{TiO}_2$ -PES is confirmed. This trend can be attributed to the very low metals (copper and titanium) leaching during removal cycle.

3.4. *E. coli* inactivation and 'OH-radical production on $\text{Cu}_x\text{O}/\text{TiO}_2$ -PES photocatalyst

In order to evaluate the effects of Cu_xO amounts (sputtering time) on TiO_2 -PES photocatalyst in the *E. coli* inactivation, Fig. 6 shows *E. coli* inactivation on $\text{Cu}_x\text{O}/\text{TiO}_2$ -PES at different sputtering times under low intensity indoor light. The fastest bacterial inactivation was seen to happen on $\text{Cu}_x\text{O}/\text{TiO}_2$ -PES photocatalyst sputtered at 80 Å, where it exhibits a total inactivation of bacteria after one hour exposition to indoor light. An increase in the sputtered time to 80 s led to increase in the bacterial inactivation rate. When Cu_xO was sputtered for longer time (100 s) the inactivation rate decreases.

The cuprous oxide exhibited high antibacterial activity, and the intrinsic activity of Cu(I) can be enhanced by the UV-vis illumination. The light illumination could facilitate electron transfer between Cu species and bacterial cells, i.e. Cu causes denaturation of bacteria protein by the electron extraction from the bacterial cells [52]. It has also been widely reported in the literature that the light irradiation leads to generate the reactive oxygen species (ROS), such as 'OH, O_2^- , and

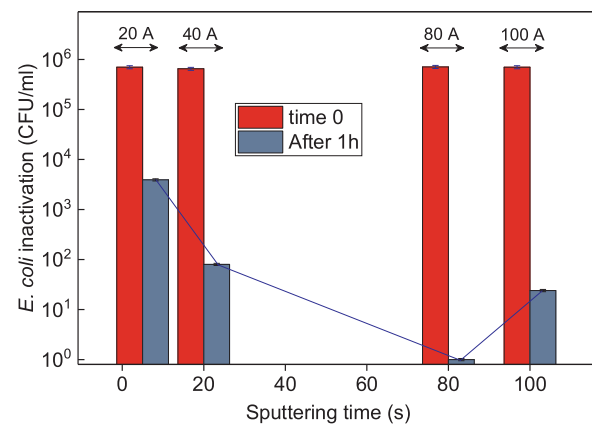


Fig. 6. *E. coli* inactivation on $\text{Cu}_x\text{O}/\text{TiO}_2$ -PES under low intensity indoor light.

H_2O_2 ...resulting in the bacterial cells inactivation. However, during our experiment, the quantification of 'OH-radicals revealed very low concentrations from all the tested samples compared to previously reported results [29]. This can be attributed to two main factors: (i) the energy levels of the present oxides in relation to the 'OH-radical potential, and (ii) the contribution of the TiO_2 under-layer in the bacterial inactivation. These two factors will be further discussed in the mechanistic section below. At this level, it should be noted that the contact between Cu(I) species and bacteria is very important for bacterial inactivation [53]. In addition, Titanium dioxide exhibits antibacterial property under UV light illumination [54]. After UV-vis light irradiation, photogenerated electron from the conduction band of cuprous oxide can be captured by Ti^{4+} in TiO_2 who is reduced to Ti^{3+} ions. The valence band of Cu_xO forms a hole center, preventing the recombination of photo-generated electrons and holes [55]. The electron trapped in Ti^{3+} can react with oxygen adsorbed on the TiO_2 surface to form O_2^- , that could transfer to H^+ for the formation of HO_2^- and 'OH. The 'OH (or/ and HO_2^- , O_2^-) can kill the bacterial cells. The hole in the TiO_2 valence band can migrate to the Cu_xO valence band, these photo-generated holes present in the VB of both semiconductors can be consumed by the oxidation of bacteria at the interface [55].

3.5. Diffuse reflectance spectroscopy (DRS), Surface oxidative states and wettability of $\text{Cu}_x\text{O}/\text{TiO}_2$ -PES

The optical properties of $\text{Cu}_x\text{O}/\text{TiO}_2$ -PES films were determined by diffuse reflectance spectroscopy (DRS) as shown in Fig. 7. Normally a weak dependence is assumed for the scattering coefficient S on the wavelength [56,57]. However, because of the relatively high scattering

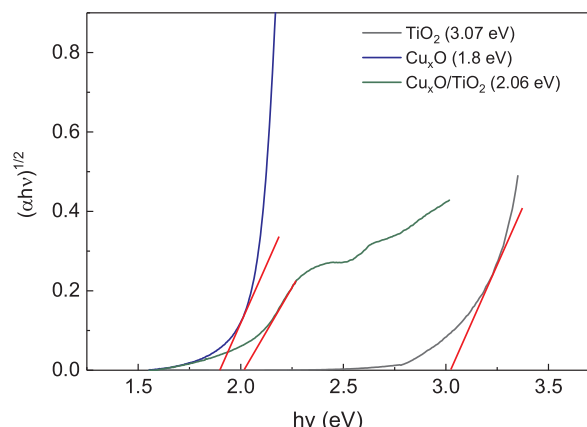


Fig. 7. Tauc's plot for band-gaps estimation of: (1) TiO_2 , (2) Cu_xO and (3) $\text{Cu}_x\text{O}/\text{TiO}_2$ deposited by HiPIMS on polyester.

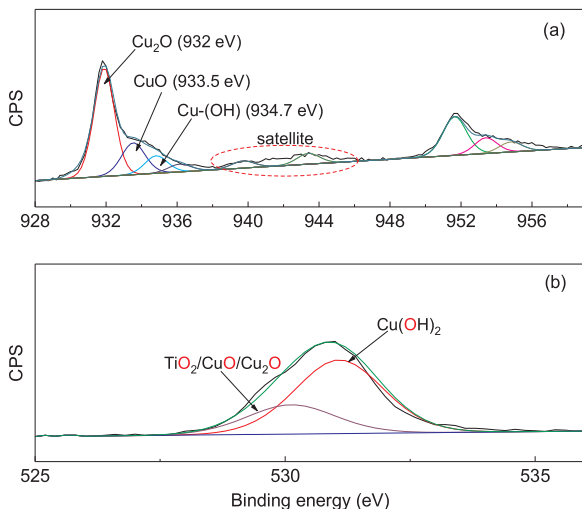


Fig. 8. XPS deconvolution of (a) Cu2p and (b) O1s at the topmost layers of Cu_xO/TiO₂-PES surface: species in direct contact with the pollutants and the bacteria.

contribution of the PES, the reflectance spectra were treated to show the real optical absorption of the sputtered Cu_xO/TiO₂-PES samples. A wide spectral range was seen for Cu_xO-PES up to almost 700 nm corresponding to a band-gap of ~1.8 eV. When Cu_xO/TiO₂ were sputtered on PES, a lower optical absorption (up to 600 nm) was observed corresponding to a band gap of 2–2.1 eV. In general, the absorption in the spectral zone 500–600 nm reflects the inter-band transition of Cu₂O-species [25]. The absorption between 600–800 nm is due to the intrinsic d-d transition induced in the Cu-oxide (especially CuO). In our case, this is observed only when we sputter Cu_xO on PES without TiO₂ under layer. The low thickness of the upper layer of Cu_xO allow the applied light to reach the TiO₂ under layer inducing photocatalytic electron/hole separation. It has been reported by Hashimoto et al., that very weak light intensities (1 μW/cm²) can induce the photocatalytic activity of Cu-TiO₂ thin films [58]. Furthermore, the same authors reported on low light intensities of 1 mW/cm² can induce bacterial inactivation at the interface of TiO₂ thin films [59].

The oxidative states at the interface Cu_xO/TiO₂-PES were investigated by XPS. The topmost layers are formed by Cu-species. The deconvolution of the Cu_xO (Cu2p3/2) peak in Fig. 8a (time zero) identifies two peaks at 932 eV and 952 eV corresponding to Cu 2p_{3/2} and Cu 2p_{1/2} respectively. A mixture of Cu⁺ and Cu²⁺ forms the Cu_xO upper layer. The co-existence of CuO and Cu₂O was recently reported by our laboratory and led to the fast Norfloxacin degradation under solar light [57]. Fig. 8a shows also the existence of two satellite peaks at 940 and 943.5 eV. Gupta and Sen reported that if excited states were taken into account, the shake-up satellites should also be considered [60]. They explained that the presence of the satellite is caused by a shake-up result. The excitation of an unpaired 3d electron to a 4s energy level. This leads to the reduction of the kinetic energy of the 2p electron by the excitation energy of the unpaired 3d electron. Thus, two peaks occur, one for the 2p excitation and the other for the combined effect of the 2p and 3d excitations. The satellite occurs generally at higher binding energies (due to the reduction of the kinetic energy).

The O1s deconvolution (Fig. 8b) shows the interdependence of Cu_xO (with its two oxidative states) and the TiO₂ under layer.

The existence of Cu(OH) at the interface of the sputtered layers reflects a strong interaction of the thin film with water molecules. To quantify the water-surface relationship, wettability of the sputtered surface was carried out using static water contact angle (CA) measurement.

The water CA on the Cu_xO/TiO₂-PES surface was investigated. The CA at time zero was 101° and dropped to 52° after 2 h irradiation. This

Table 2

Oxidative states changes as determined by XPS peaks areas within indoor light irradiation for 2 h.

	Cu ⁺	Cu ²⁺
Cu _x O/TiO ₂ -PES Time zero	32.4	77.6
Cu _x O/TiO ₂ -PES After 2 h irradiation	48	52

can be attributed to the surface chemistry (especially OH-groups) and to the porous micro/nanostructured PES surface allowing the water droplet to vanish. Furthermore, this photo-switching behavior can be attributed to the physical adsorption of oxygen molecules on the topmost layer of the Cu_xO. The wettability of a flat surface can obey to the Wenzel model. This model is not sufficient when the surface composition is heterogeneous. The Cassie's law (based on the Cassie-Baxter equation, eq.1) can explain the wettability of these surfaces [61]:

$$\cos(\theta^*) = r_f f \cos(\theta_Y) + f - 1 \quad (1)$$

Where: r_f is the roughness ratio of the wet surface area and f is the fraction of solid surface area wet by the liquid. When $f = 1$ and $r_f = r$, the Cassie-Baxter equation is equivalent to the Wenzel equation. A wetting equilibrium on the rough PES surface is understood based on the competition between the hydrophobic surface and the photo-catalytically induced hydrophilicity (52° after 2 h illumination). This involves oxidative states changes, as it was previously reported [62]. Table 2 shows the oxidative states changes of Cu_xO at the interface with VOCs and bacteria in ambient air.

It is expected that Cu⁺ can attain the d10 configuration by losing one electron from the s-subshell. Nonetheless, because it has fully filled d-orbital, it is stable. However, in aqueous medium (in our case, bacterial suspension) or with moist air (in our case, indoor air), Cu⁺ is unstable and tends to disproportionate leading to the formation of Cu²⁺, which presents incompletely filled d-orbital (d9 configuration). This leads to fast restoration of the surface reestablishing the initial oxidative states prior to the illumination.

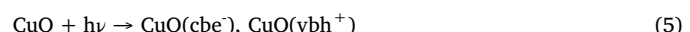
3.6. Suggested mechanism for the Cu_xO/TiO₂ pollutants degradation and bacterial inactivation

The XPS results suggest the reaction sequence on the sample surface of the sputtered catalysts, which are at the interface with the VOCs and the bacteria, as:



The pattern of the Cu (and Ti) sputtered on the PES surface is complicated by the surface diffusion controlling the charge transport between Cu(II)/Cu(I) and Ti on the PES surface. In the topmost layers, the Cu⁰, Cu₂O, CuO and TiO₂ present motions leading to agglomerates presenting a different collective diffusion [63].

The distinct kinetics of bacterial inactivation and VOCs degradation times can be attributed to the intrinsic conduction band (cb) and valence band (vb) positions of CuO and Cu₂O. On these bases, the vectorial charge displacement/flow is shown for both oxides in Fig. 9a. The CuO present a band-gap (of 1.7 eV), cb (~0.3 eV) and vb (~1.4 eV) while direct band-gap of Cu₂O p-type presents a band-gap of 2.1 eV, cb (~1.4 eV) and vb (~0.7 eV). This can be summarized in the equations below:



Under photon energies exceeding the CuO band-gap, the cbe-electron could either react directly with the O₂ forming O₂[−] or reduce the Cu²⁺ to Cu⁺ as noted below and as shown in Fig. 9a:

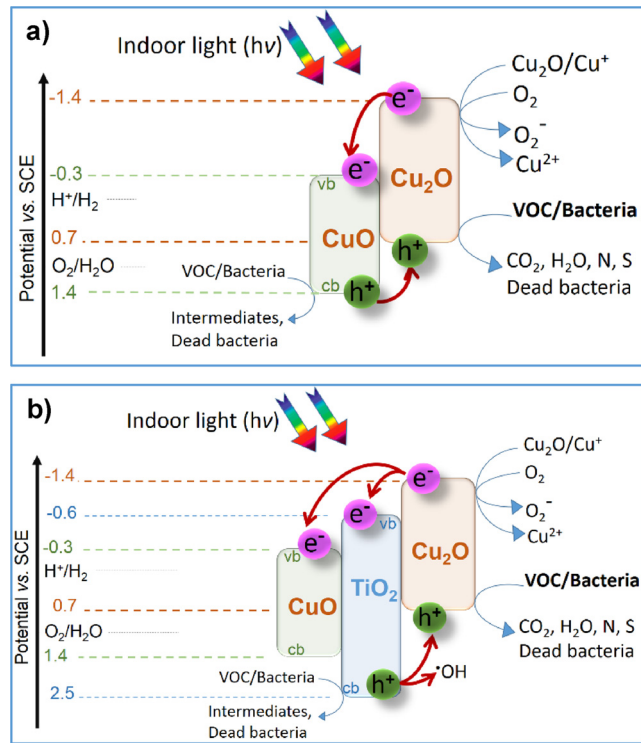
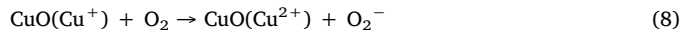
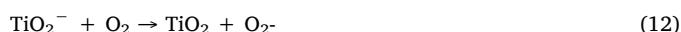
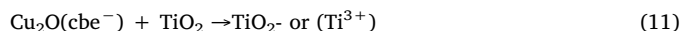
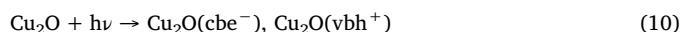


Fig. 9. Proposed mechanisms of action of the prepared photocatalyst: (a) if we consider just Cu_xO interface, (b) if we consider a photocatalytic intervention of the TiO₂ under layer.

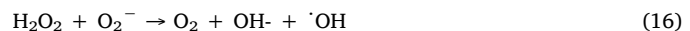
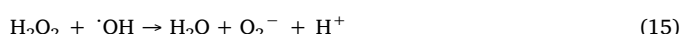
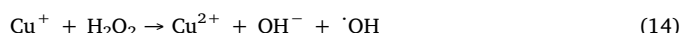


Since the Cu_xO topmost layer is transparent allowing the light to reach TiO₂, the photocatalytic reactions of Cu_xO/TiO₂-PES under light can be summarized below by Eqs. (10–13). The highly mobile electrons transfer from Cu_xOcb to the TiO₂cb as shown in Fig. 9b. The vbh⁺ will react leading to the observed bacterial inactivation and/or VOC degradation.



However, this mechanism presented in Fig. 9b is low probable because of the very low amount of OH-radical detected by fluorescence experiment.

Many research groups reported the Fenton-like reaction allowing the generation of OH-radical on copper surfaces [64] (see Eq. 14). Furthermore, some other researchers went further by combining/associating the Fenton-like reaction to the Haber-Weiss cycle (Eqs. 15 and 16) leading to the generation of OH-radicals from H₂O₂, which in turn activates the copper Fenton-like reaction. Although Haber-Weiss reaction has long been studied and revived in different contexts, this association is still hypothetical and requires deep systematic investigation.



Sputtered materials were reported to degrade organic compounds [65]. In the present study, the prepared material is tested for VOC removal and bacterial inactivation. This comprises ROS generation and their diffusion/migration in different media (liquid, suspension, air). This challenges systematic investigation of the possible photo-generated charges diffusion over different matrices.

4. Conclusion

This report presents the testing of an innovative uniform and stable sputtered Cu_xO/TiO₂-PES photocatalyst prepared at low temperature by high power impulse magnetron sputtering. This is the first report on uniform coatings of Cu/CuO on PES leading to the degradation of indoor air VOCs concomitant with an antibacterial activity. Two concentrate VOC models were removed at the interface of Cu_xO/TiO₂-PES. Moreover, a stable removal performance of the chloroform by the Cu_xO/TiO₂-PES samples was observed during repetitive recycling under visible irradiation. This catalyst feature shows an excellent catalytic stability and presents a promising potential for the application in air treatment. The Cu_xO/TiO₂-PES photocatalyst exhibits a high antibacterial activity, which attained a total bacterial inactivation within 2 h on Cu_xO/TiO₂-PES sputtered at 80 A. This makes the Cu_xO/TiO₂ surfaces presented in the present study have promising applications in Lotus effect self-cleaning coatings for hospital textiles.

Declaration of Competing Interest

The authors declare that they have no known competing financial interests or personal relationships that could have appeared to influence the work reported in this paper.

Acknowledgements

S.R. would like to thank Prof. H. Hofmann for the support during the TEM and XPS experiment, a special thank goes to Prof. C. Pulgarin for the bio-lab facility and the support of the Institute of Physics (iPhys, EPFL) is deeply acknowledged.

References

- [1] <http://www.developpement-durable.gouv.fr/Valeurs-guides-de-l-air-interieur.html>.
- [2] ADEME, Qualification énergétique et sanitaire des systèmes d'épuration intégrés aux réseaux de ventilation, (2015).
- [3] Directive (EU) 2016/2284 du Parlement Européen et du Conseil du 14 décembre, concernant la réduction des émissions nationales de certains polluants atmosphériques modifiant la directive 2003/35/CE et abrogeant la directive 2001/81/CE, JOUE, 2016 17.12.2016; L344/1.
- [4] N.E. Klepeis, W.C. Nelson, W.R. Ott, J.P. Robinson, A.M. Tsang, P. Switzer, J.V. Behar, S.C. Hern, W.H. Engelmann, The National Human Activity Pattern Survey (NHAPS): a resource for assessing exposure to environmental pollutants, *J. Expo. Anal. Environ. Epidemiol.* 11 (2001) 231–252.
- [5] G.R. Parmar, N.N. Rao, Emerging control technologies for volatile organic compounds, *Crit. Rev. Environ. Sci. Technol.* 39 (2009) 41–78.
- [6] S. Gharib-Abou Ghaida, A.A. Assadi, G. Costa, A. Bouzaza, D. Wolbert, Association of surface dielectric barrier discharge and photocatalysis in continuous reactor at pilot scale: butyraldehyde oxidation, by-products identification and ozone valorization, *Chem. Eng. J.* 292 (15) (2016) 276–283.
- [7] NOx—How Nitrogen Oxides Affect the Way We Live and Breathe, EPA-456/F-98-005, United States Environmental Protection Agency, 1998 September.
- [8] J. Matos, A. Garcia, J.-M. Chovelon, C. Ferronato, Combination of adsorption on activated carbon and oxidative photocatalysis on tio2 for gaseous toluene remediation, *Open Mater. Sci. J.* 4 (2010) 23–25.
- [9] M. Wang, A. Lawal, P. Stephenson, J. Sidders, C. Ramshawa, Post-combustion CO₂ capture with chemical absorption: a state-of-the-art review, *Chem. Eng. Res. Des.* 89 (2011) 1609–1624.
- [10] A.A. Assadi, A. Bouzaza, I. Soutrel, P. Petit, K. Medimagh, D. Wolbert, A study of pollution removal in exhaust gases from animal quartering centers by combining photocatalysis with surface discharge plasma: from pilot to industrial scale, *Chem. Eng. Process. Process. Intensif.* 111 (2017) 1–6.
- [11] A.A. Assadi, A. Bouzaza, C. Vallet, D. Wolbert, Use of DBD plasma, photocatalysis,

and combined DBD plasma/photocatalysis in a continuous annular reactor for isovaleraldehyde elimination–synergetic effect and byproducts identification, *Chem. Eng. J.* 254 (2014) 124–132.

[12] M. Guillerm, A.A. Assadi, A. Bouaza, D. Wolbert, Removal of gas-phase ammonia and hydrogen sulfide using photocatalysis, non-thermal plasma, and combined plasma and photocatalysis at pilot scale, *Environ. Sci. Pollut. Res. - Int.* 21 (2014) 13127–13137.

[13] J. Palau, J.M. Penya-Roja, C. Gabaldon, F.J. Alvarez-Hornos, V. Martinez-Soria, Effect of pre-treatments based on UV photocatalysis and photo-oxidation on toluene biofiltration performance, *J. Chem. Technol. Biotechnol.* 87 (2011) 65–72.

[14] A.A. Assadi, A. Bouaza, D. Wolbert, P. Petit, Isovaleraldehyde elimination by UV/TiO₂ photocatalysis: comparative study of the process at different reactors configurations and scales, *Environ. Sci. Pollut. Res. - Int.* 21 (2016) 11178–11188.

[15] V. Binas, D. Venieri, D. Kotzias, G. Kiriakidis, Modified TiO₂ based photocatalysts for improved air and health quality, *J. Mater.* 3 (2017) 3–16.

[16] L. Zhong, F. Haghishat, Photocatalytic air cleaners and materials technologies - Abilities and limitations, *Build. Environ.* 91 (2015) 191–203.

[17] D. Farhanian, F. Haghishat, Photocatalytic oxidation air cleaner: identification and quantification of by-products, *Build. Environ.* 72 (2014) 34–43.

[18] A.A. Assadi, A. Bouaza, D. Wolbert, P. Petit, Isovaleraldehyde elimination by UV/TiO₂ photocatalysis: comparative study of the process at different reactors configurations and scales, *Environ. Sci. Pollut. Res. - Int.* 21 (2014) 11178–11188.

[19] A.A. Assadi, A. Bouaza, D. Wolbert, Photocatalytic oxidation of trimethylamine and Isovaleraldehyde in an annular reactor: influence of the mass transfer and the relative humidity, *J. Photochem. Photobiol. A: Chem.* 236 (2012) 61–69.

[20] A.A. Assadi, J. Palau, A. Bouaza, J. Penya-Roja, V. Martinez-Soria, D. Wolbert, Abatement of 3-methylbutanal and trimethylamine with combined plasma and photocatalysis in a continuous planar reactor, *J. Photochem. Photobiol. A: Chem.* 282 (2014) 1–8.

[21] A. Bouaza, C. Vallet, A. Laplanche, Photocatalytic degradation of some VOCs in the gas phase using an annular flow reactor: determination of the contribution of mass transfer and chemical reaction steps in the photo-degradation process, *J. Photochem. Photobiol. A: Chem.* 177 (2006) 212–217.

[22] A.A. Assadi, J. Palau, A. Bouaza, D. Wolbert, A continuous air reactor for photocatalytic degradation of 3-methylbutanal: effect of different operating parameters and chemical degradation pathway, *Chem. Eng. Res. Des.* 91 (2013) 1307–1316.

[23] W. Abou Saoud, A.A. Assadi, M. Guiza, A. Bouaza, W. Aboussaoud, A. Ouederni, I. Soutrel, D. Wolbert, S. Rtimi, Study of synergetic effect, catalytic poisoning and regeneration using dielectric barrier discharge and photocatalysis in a continuous reactor: abatement of pollutants in air mixture system, *Appl. Catal. B* 213 (2017) 53–61.

[24] A.Y. Shan, T.I.M. Ghazi, S.A. Rashid, Immobilization of titanium dioxide onto supporting materials in heterogeneous photocatalysis: a review, *Appl. Catal. A Gen.* 389 (2010) 1–8.

[25] M. Pachoalino, J. Kiwi, W. Jardim, Gas phase photocatalytic decontamination using polymer supported TiO₂, *Appl. Catal. B* 68 (2006) 68–73.

[26] W. Elfalleh, A.A. Assadi, A. Bouaza, D. Wolbert, J. Kiwi, S. Rtimi, Innovative and stable TiO₂ supported catalytic surfaces removing aldehydes under UV-light irradiation, *J. Photochem. Photobiol. A: Chem.* 343 (2017) 96–102.

[27] H. Zeghoudi, N. Khellaf, A. Amrane, H. Djelal, W. Elfalleh, A.A. Assadi, S. Rtimi, Photocatalytic performance of TiO₂ impregnated polyester for the degradation of Reactive Green 12: implications of the surface pretreatment and the microstructure, *J. Photochem. Photobiol. A: Chem.* 346 (2017) 493–501.

[28] S. Rtimi, O. Baghriche, R. Sanjines, C. Pulgarin, M. Bensimon, J. Kiwi, TiON and TiON-Ag sputtered surfaces leading to bacterial inactivation under indoor actinic light, *J. Photochem. Photobiol. A: Chem.* 256 (2013) 52–63.

[29] S. Rtimi, O. Baghriche, C. Pulgarin, J.-C. Lavanchy, J. Kiwi, Growth of TiO₂/Cu films by HiPIMS for accelerated bacterial loss of viability, *Surf. Coat. Technol.* 232 (2013) 804–813.

[30] S. Rtimi, M. Pascu, R. Sanjines, C. Pulgarin, M. Ben-Simon, A. Houas, J.-C. Lavanchy, J. Kiwi, ZrNO–Ag co-sputtered surfaces leading to *E. coli* inactivation under actinic light: evidence for the oligodynamic effect, *Appl. Catal. B* 138–139 (2013) 113–121.

[31] Z. Shayegan, C.S. Lee, F. Haghishat, TiO₂ photocatalyst for removal of volatile organic compounds in gas phase—a review, *Chem. Eng. J.* 334 (2018) 2408–2439.

[32] T.D. Pham, B.K. Lee, D. Pham-Cong, Advanced removal of toluene in aerosol by adsorption and photocatalytic degradation of silver-doped TiO₂/PU under visible light irradiation, *RSC Adv.* 6 (2016) 25346–25358.

[33] H. Lin, W. Deng, T. Zhou, S. Ning, J. Long, X. Wang, Iodine-modified nanocrystalline titania for photo-catalytic antibacterial application under visible light illumination, *Appl. Catal. B* 176–177 (2015) 36–43.

[34] Y. Zhang, Chen Lin, Qun Lin, Y. Jin, Y. Wang, Z. Zhang, H. Lin, J. Long, X. Wang, CuI-BiOI/Cu film for enhanced photo-induced charge separation and visible-light antibacterial activity, *Appl. Catal. B* 235 (2018) 238–245.

[35] S. Ning, H. Lin, Y. Tong, X. Zhang, Q. Lin, Y. Zhang, J. Long, X. Wang, Dual couples Bi metal depositing and Ag@AgI islanding on BiOI 3D architectures for synergistic bactericidal mechanism of *E. coli* under visible light, *Appl. Catal. B* 204 (2017) 1–10.

[36] T. Ochiai, T. Hoshi, H. Slimen, K. Nakata, T. Murakami, H. Tatejima, Y. Koide, A. Houas, T. Horie, Y. Moritobe, A. Fujishima, Fabrication of a TiO₂ nanoparticles impregnated titanium mesh filter and its application for environmental purification, *Catal. Sci. Technol.* 1 (2011) 1324–1327.

[37] S. Rtimi, S. Giannakis, R. Sanjines, C. Pulgarin, M. Bensimon, J. Kiwi, Insight on the photocatalytic bacterial inactivation by co-sputtered TiO₂–Cu in aerobic and anaerobic conditions, *Appl. Catal. B* 182 (2016) 277–285.

[38] J. Mathews, Epitaxial Growth Part B, IBM Thomas Watson Research Center, Academic Press, New York, 1975, pp. 382–436.

[39] M.I. Mejia, J.M. Marin, G. Restrepo, L.A. Rio, C. Pulgarin, J. Kiwi, Preparation, testing and performance of TiO₂/polyester for the degradation of gaseous methanol, *Appl. Catal. B* 94 (2010) 166–172.

[40] S. Rtimi, J. Nesic, C. Pulgarin, R. Sanjines, M. Bensimon, J. Kiwi, Effect of surface pretreatment of TiO₂ films on interfacial processes leading to bacterial inactivation in the dark and under light irradiation, *Interface Focus* 5 (2015) 20140046.

[41] R.A. Jelil, A review of low-temperature plasma treatment of textile materials, *J. Mater. Sci.* 50 (2015) 5913–5943.

[42] K. Sarakinos, J. Alami, S. Konstantinidis, High power pulsed magnetron sputtering: a review on scientific and engineering state of the art, *Surf. Coat. Technol.* 204 (2010) 1661–1684.

[43] S. Rtimi, Indoor light enhanced photocatalytic ultra-thin films on flexible non-heat resistant substrates reducing bacterial infection risks, *Catalysts* 7 (2017) 57.

[44] S. Rtimi, S. Konstantinidis, N. Britun, M. Bensimon, I. Khmel, V. Nadtchenko, Extracellular bacterial inactivation proceeding without Cu-ion release: drastic effects of the applied plasma energy on the performance of the Cu-polyester (PES) samples, *Appl. Catal. B: Environ.* 239 (2018) 245–253.

[45] N. Britun, M. Palmucci, S. Konstantinidis, R. Snyders, Particle visualization in high-power impulse magnetron sputtering. II. Absolute density dynamics, *J. Appl. Phys.* 117 (2015) 163303.

[46] S. Konstantinidis, J.P. Dauchot, M. Hecq, Titanium oxide thin films deposited by high-power impulse magnetron sputtering, *Thin Solid Films* 515 (2006) 1182–1186.

[47] N. Britun, T. Minea, S. Konstantinidis, R. Snyders, Plasma diagnostics for understanding the plasma-surface interaction in HiPIMS discharges: a review, *J. Phys. D Appl. Phys.* 47 (2014) 224001.

[48] J. Kiwi, C. Pulgarin, Innovative self-cleaning and bactericide textiles, *Catal. Today* 151 (2010) 2–7.

[49] J. Kiwi, C. Pulgarin, Self-cleaning textiles modified by TiO₂ and bactericide textiles modified by Ag and Cu, *Self-Cleaning Mater. Surf.: A Nanotechnol. Approach* (2013) 203–227.

[50] M.I. Mejia, J.M. Marin, G. Restrepo, C. Pulgarin, E. Mielczarski, J. Mielczarski, J. Kiwi, Innovative UVC light (185 nm) and radio-frequency-plasma pretreatment of nylon surfaces at atmospheric pressure and their implications in photocatalytic processes, *ACS Appl. Mater. Interfaces* 1 (2009) 2190–2198.

[51] M.I. Mejia, J.M. Marin, G. Restrepo, C. Pulgarin, E. Mielczarski, J. Mielczarski, J. Kiwi, Self-cleaning modified TiO₂-cotton pretreated by UVC-light (185 nm) and RF-plasma in vacuum and also under atmospheric pressure, *Appl. Catal. B* 91 (2009) 481–488.

[52] K. Sunada, M. Minoshima, K. Hashimoto, Highly efficient antiviral and antibacterial activities of solid-state cuprous compounds, *J. Hazard. Mater.* 235 (2012) 265–270.

[53] O. Baghriche, S. Rtimi, C. Pulgarin, R. Sanjines, J. Kiwi, Innovative TiO₂/Cu nano-surfaces inactivating bacteria in the minute range under low-intensity actinic light, *ACS Appl. Mater. Interfaces* 4 (2012) 5234–5240.

[54] Li H, Q. Cui, B. Feng, J. Wang, X. Lu, J. Weng, Antibacterial activity of TiO₂ nanotubes: influence of crystal phase, morphology and Ag deposition, *Appl. Surf. Sci.* 284 (2013) 179–183.

[55] L. Xiong, F. Yang, L. Yan, N. Yan, X. Yang, M. Qiu, Y. Yu, Bifunctional photocatalysis of TiO₂/Cu₂O composite under visible light: Ti³⁺ in organic pollutant degradation and water splitting, *J. Phys. Chem. Solids* 72 (2011) 1104–1109.

[56] C. Auer, W. Grieber, B. Jahn, *Industrial Inorganic Pigments*, Wiley Verlag, Weinheim, 2005.

[57] G. Mamba, C. Pulgarin, J. Kiwi, M. Bensimon, S. Rtimi, Synchronic coupling of Cu₂O(p)/Cu₀(n) semiconductors leading to Norfloxacin degradation under visible light: kinetics, mechanism and film surface properties, *J. Catal.* 353 (2017) 133–140.

[58] K. Sunada, T. Watanabe, K. Hashimoto, Bactericidal activity of copper-deposited TiO₂ thin film under weak UV light illumination, *Environ. Sci. Technol.* 37 (2003) 4785–4789.

[59] K. Sunada, T. Watanabe, K. Hashimoto, Studies on photokilling of bacteria on TiO₂ thin film, *J. Photochem. Photobiol. A: Chem.* 156 (2003) 227–233.

[60] R.P. Gupta, S.K. Sen, Calculation of multiplet structure of core p-vacancy levels, II, *Phys. Rev. B* 12 (1975) 15.

[61] A. Marmur, Wetting of hydrophobic rough surfaces: to be heterogeneous or not to be, *Langmuir* 19 (2003) 8343–8348.

[62] S. Rtimi, C. Pulgarin, R. Sanjines, J. Kiwi, Innovative semi-transparent nano-composite films presenting photo-switchable behavior and leading to a reduction of the risk of infection under sunlight, *RSC Adv.* 3 (2013) 16345–16348.

[63] J. Venable, G. Price, J.B. Mathews (Ed.), *Epitaxial Growth Part B*, Academic Press, New York, 1975, pp. 382–423 Chapter 4.

[64] O. Baghriche, S. Rtimi, C. Pulgarin, J. Kiwi, Polystyrene CuO/Cu₂O uniform films inducing MB-degradation under sunlight, *Catal. Today* 284 (2017) 77–83.

[65] H. Zeghoudi, A.A. Assadi, N. Khellaf, H. Djelal, A. Amrane, S. Rtimi, Photocatalytic performance of Cu_xO/TiO₂ deposited by HiPIMS on polyester under visible light LEDs: oxidants, ions effect, and reactive oxygen species investigation, *Materials* 12 (2019) 412.